

COMPUTER STUDY OF WAVE PROPAGATION, BEAM LOADING AND BEAM BLOWUP IN THE SLAC ACCELERATOR †

R. Helm

Stanford Linear Accelerator Center, Stanford University, Stanford California

Introduction

The classical type of beam blowup or pulse shortening which is observed in many short, high-current electron linacs<sup>1,2</sup> has been convincingly identified<sup>2,4</sup> as a regenerative interaction between the beam and the HEM<sub>11</sub> deflecting mode,<sup>3</sup> which is the next pass band above the accelerating mode. The backward wave characteristic usually associated with the deflecting mode supplies a prompt feedback mechanism which can greatly enhance the rate of transient buildup. Several analyses of the starting current threshold and transient behavior of this phenomenon<sup>5,6,7</sup> and its analogue in proton linacs<sup>8</sup> have been published. The starting currents are typically of the order of a few hundred milliamperes to a few amperes.

In multi-section machines another possibility suggests itself; namely, an initial transverse modulation of the beam might be amplified, by the same type of HEM<sub>11</sub> mode interaction, in each accelerator section. The many slight successive amplifications could lead to instability even at beam currents considerably below the threshold for the free oscillations. In fact it has been observed in high current multi-section linacs such as the DESY injector<sup>9</sup> and the Kharkov electron linac<sup>10</sup> that the pulse shortening threshold decreases with distance down the machine.

The beam blowup observed at SLAC, as reported by Farinholt et al.,<sup>11</sup> occurs at a frequency within the HEM<sub>11</sub> pass band but at currents at least on order of magnitude lower than the threshold for the regenerative oscillation. Evidently then this is a case of the cascaded amplifier mechanism.

At the time the present work was begun, the author thought that a formulation of the blowup interaction in the SLAC structure would have to include a detailed description of the transient wave propagation. This is a complicated problem for several reasons: First, the structure is tapered to produce constant gradient in the accelerating mode.<sup>12</sup> In the deflecting mode, as a result, there is a band of frequencies about 200 MHz wide, within which the phase velocity is synchronous with the beam somewhere in the 10 ft. section. Second, the synchronous frequency is very close to the  $\pi$ -mode where the dispersion is so great that a simple description of wave propagation, in terms of a well-defined group velocity, is not valid.

In order to represent the dispersive effects at least approximately, the coupled-resonator model<sup>13-17</sup> of the wave propagation was adopted. Because of the complexity of the problem, a computer solution was undertaken.

As an intermediate goal in the development of a computer program, the case of wave propagation and beam loading in the accelerating mode was treated.

At about this time real beam blowup was discovered at SLAC. It was soon realized that the essential properties of the blowup could be described in a simple way without using the coupled-resonator model, i.e., by representing an entire accelerator section as a single short resonant cavity.<sup>18,19</sup> However, it still seemed worthwhile to continue the present approach. The

blowup version of the computer program can simulate both the single cavity and the coupled-resonator models.

In the present work the affects of other propagating modes such as the HEM<sub>21</sub> (quadrupole) and HEM<sub>12</sub> (higher dipole), and non-propagating fields (wake-field effect) are not considered.

Formulation

Coupled Resonator Wave Equation

We wish to express the wave propagation and beam interaction in a chain of coupled cavities without imposing explicit normal-mode constraints. Thus rather than employing an expansion in normal modes, we assume that the vector potential in the nth cavity (see Fig. 1) may be expressed, in Fourier-transform representation, by\*

$$\vec{A} = A_n(\omega) \vec{\psi}_n(\vec{r}; \omega) \quad (1)$$

where  $\vec{\psi}_n$  is a wave function, characteristic to the nth cavity.\*\* It is assumed that space charge and scalar potentials may be neglected. The electric and magnetic fields are defined in the usual convention by\*\*\*

$$\vec{E} = -\frac{i\omega}{c} \vec{A}, \quad \vec{B} = \nabla \times \vec{A},$$

and  $\vec{A}$  is a solution of the vector wave equation

$$\nabla \times \nabla \times \vec{A} - \frac{\omega^2}{c^2} \vec{A} = \frac{4\pi}{c} \vec{J}$$

The coupled resonator wave equation, which is found by appropriate operation on the vector wave equation, may be stated as (see e.g., Refs. 14 and 15)

$$\begin{aligned} (\omega_n^2 + 2i\omega\alpha_n - \omega^2) A_n - (K_n^{n-1} A_{n-1} + K_n^{n+1} A_{n+1}) \\ = \frac{4\pi c}{u_n} \int_{\text{cav.}} \vec{\psi}_n^* \cdot \vec{J}_n \, dV \end{aligned} \quad (2)$$

\* The Fourier transformation is used in the operational sense:

$$F(\omega) = \frac{1}{2\pi} \int_{-\infty}^{\infty} f(t) e^{-i\omega t} \, dt,$$

$$f(t) = \int_c F(\omega) e^{i\omega t} \, d\omega.$$

In order to conserve on definitions, it will be convenient to use  $A(\omega)$  to designate the Fourier transform of  $A(t)$ , etc.

\*\* More precisely,  $\vec{A}$  should be expressed as a sum over a set of transversely orthogonal modes  $\vec{\psi}_{mn}$ . Only one transverse mode need be considered at a time, so the mode index  $m$  is omitted.

\*\*\* Gaussian Units are used.

where  $\omega_n$  is a characteristic parameter of the nth cavity,

$$\alpha_n = \frac{\omega_n}{2Q_n} = \text{the loss factor}$$

$K_n^{n\pm 1}$  is a parameter which expresses the coupling between the n±1 and nth cavities,

$\vec{J}_n$  is the beam current through the cavity, and

$$u_n = \int_{\text{cav.}} |\psi_n|^2 dV = \text{integral of } |\psi|^2 \text{ over the cavity volume}$$

The parameters of Eq. (2) are given formally by\*

$$\omega_n^2 = \frac{c^2}{u_n} \int_{\text{cav.}} |\nabla \times \vec{\psi}_n|^2 dV$$

$$K_n^{n\pm 1} = \frac{c^2}{u_n} \int_{\text{hole}} [\vec{\psi}_n^* \times (\nabla \times \vec{\psi}_{n\pm 1})] \cdot \vec{ds}$$

$$\alpha_n \cong \frac{c^2 \delta}{4\omega} \frac{1}{u_n} \int_{\text{wall}} |\nabla \times \vec{\psi}_n|^2 ds$$

where  $\delta = \sqrt{c/2\pi\omega\sigma}$  = the skin depth. Fortunately these parameters may be related to experimentally measurable quantities, as will be seen below, so that detailed solution of the vector wave equation is not needed.

If we assume that the beam current is traveling in the +z direction at velocity v, so that in the time domain

$$J_{zn}(\vec{r}', t) = J(\vec{r}', t - \int_0^z dz/v) \quad (3)$$

$$J_{xn} \cong J_{yn} \cong 0$$

then the Fourier transformed current density is

$$J_{zn}(\vec{r}', \omega) = J(\vec{r}', \omega) e^{-i\omega(t_n + \xi/v_n)} \quad (3')$$

$$\text{where } t_n = \int_0^{z_n} dz/v, \quad (4)$$

$v_n$  is the average particle velocity at the nth cavity, and  $\xi$  is the longitudinal displacement relative to the center of the cavity. Equation (2) then becomes

$$\begin{aligned} (\omega_n^2 + 2i\omega\alpha_n - \omega^2) A_n - (K_n^{n-1} A_{n-1} + K_n^{n+1} A_{n+1}) \\ = \frac{4\pi c}{u_n} e^{-i\omega t_n} \int_{\text{cav.}} \vec{\psi}_{zn}^* J e^{-i\omega \xi/v_n} dV \end{aligned} \quad (5)$$

### Dispersion Equation

Consider now the homogeneous part of the coupled resonator wave equation for a structure in which the parameters are longitudinally constant ( $\omega_n, \alpha_n, K_n^{n\pm 1}$  independent of n):

$$(\omega_0^2 + 2i\omega\alpha - \omega^2) A_n - K(A_{n-1} + A_{n+1}) = 0 \quad (6)$$

where the physically plausible assumption (reciprocity)

$$K_n^{n\pm 1} = K_{n\pm 1}^n$$

has been used.

Equation (6) has solutions of the form

$$A_n \sim e^{\pm ink\ell}$$

where

$$\omega_0^2 + 2i\omega\alpha - \omega^2 = 2K \cos k\ell \quad (7)$$

and  $k\ell$  is the complex phase shift per cavity.

Equation (7) is frequently used in describing the dispersion in simple coupled resonator structures; the coupling parameter K is essentially proportional to  $\omega^2$  for "magnetic" coupling and independent of  $\omega$  for "electric" coupling.<sup>15</sup>

The "pass band," for which  $k\ell$  is predominantly real, is in the range

$$\sqrt{\omega_0^2 - 2K} \lesssim |\omega| \lesssim \sqrt{\omega_0^2 + 2K},$$

if we make the usual small-loss assumption

$$\alpha = \frac{\omega_0}{2Q} \ll \omega_0.$$

It will be convenient to make the additional assumptions:

(1) that the pass-band is narrow, i.e.

$$|K/\omega_0| \ll \omega_0.$$

(2) that we only need to consider frequency components in or near the pass-band; e.g.,

$$|\omega - \omega_0| \sim |K/\omega_0| \ll \omega_0.$$

Because of the last assumption, we take the parameters  $\omega_0, \alpha,$  and  $K$  to be independent of frequency over the frequency band of interest.

The dispersion equation now may be written in the approximate form

$$\omega_0 + i\alpha - \omega \cong \Omega \cos k\ell \quad (8)$$

where  $\Omega = \text{half-bandwidth} \cong \frac{K}{\omega_0}$ .

Equation (8) will be recognized as precisely the dispersion relation used by Leiss and Schrack<sup>20</sup> in describing transient phenomena in Linac waveguides. The equivalent Brillouin diagram is shown in Fig. 2.

Thus to the extent that Eq. (8) represents the actual dispersion curve, the parameters  $\omega_0$  and  $\Omega$  may be determined from the experimental Brillouin diagram. The loss parameter  $\alpha$  (or  $Q$ ) is commonly

\* See, e.g., Slater<sup>14</sup> and Bevensee.<sup>15</sup>

found e.g., either by resonance width or attenuation measurements.

### Simplified Wave Equation

If we apply the approximations of the previous section to Eq. (5), the Fourier transformed wave equation becomes

$$\begin{aligned} & (\omega_n + i\alpha_n - \omega)A_n - \frac{1}{2}(\Omega_n^{n-1}A_{n-1} + \Omega_n^{n+1}A_{n+1}) \\ & = \frac{2\pi c}{\omega_n' u_n} e^{-i\omega_n t} \int_{\text{cav.}} \psi_{zn}^* J e^{-i\omega_n' \xi / v_n} dV \end{aligned} \quad (9)$$

where  $\omega_n'$  is some constant reference frequency in or near the pass-band;

$$\omega_n' \equiv \frac{1}{2}(\omega_n + \omega') \quad ;$$

$$\Omega_n^{n\pm 1} \equiv \frac{1}{\omega_n'} K_n^{n\pm 1} \quad ;$$

and we assume that  $\alpha_n$ ,  $\omega_n$ ,  $\Omega_n^{n\pm 1}$ , and  $\vec{\psi}_n$  are essentially independent of  $\omega$  (i.e., the leading term in an expansion about  $\omega'$  should be used).

We may now transform to the time domain by identifying the operator  $i\omega$  as  $\partial/\partial t$ ; the result is

$$\begin{aligned} & \left(\frac{\partial}{\partial t} + \alpha_n - i\omega_n\right)A_n + \frac{i}{2} \left(\Omega_n^{n-1}A_{n-1} + \Omega_n^{n+1}A_{n+1}\right) \\ & = \frac{2\pi c}{i\omega_n' u_n} \int_{\text{cav.}} \psi_{zn}^* J(\vec{r}', t-t_n) e^{-i\omega_n' \xi / v_n} dV \end{aligned} \quad (10)$$

In describing the interaction of the wave with a beam of particles it will be convenient to introduce the local time defined by

$$\tau = t - \int_0^{z_n} dz/v = t - t_n \quad (11)$$

Then the wave equation may be written

$$\begin{aligned} & \left(\frac{\partial}{\partial t} + \alpha - i\omega_n\right)A_n(\tau) \\ & + \frac{i}{2} \left\{ \Omega_n^{n-1} A_{n-1}(\tau + \ell/v_n) + \Omega_n^{n+1} A_{n+1}(\tau - \ell/v_n) \right\} \\ & = \frac{2\pi c}{i\omega_n' u_n} \int_{\text{cav.}} \psi_{zn}^* J(\vec{r}', \tau) e^{-i\omega_n' \xi / v_n} dV \end{aligned} \quad (12a)$$

Alternately we could retain the quadratic form of the dispersion Eq. (7) and obtain in an analogous

way

$$\begin{aligned} & \left(\frac{\partial^2}{\partial \tau^2} + 2\alpha_n \frac{\partial}{\partial \tau} + \omega_n'^2\right)A_n(\tau) \\ & - \omega_n' \left\{ \Omega_n^{n-1} A_{n-1}\left(\tau + \frac{\ell}{v_n}\right) + \Omega_n^{n+1} A_{n+1}\left(\tau - \frac{\ell}{v_n}\right) \right\} \\ & = \frac{4\pi c}{u_n} \int_{\text{cav.}} \psi_{zn} J(\vec{r}', \tau - \xi/v_n) dV \end{aligned} \quad (12b)$$

where now a real rather than complex representation is employed. The assumption that the parameters  $\alpha_n$ ,  $\omega_n$ ,  $\Omega_n^{n\pm 1}$ , etc., are independent of frequency is still implied, so that the wave equation in the form (12b) is also only a quasi-transient approximation, valid in a frequency band not too far from the reference frequency  $\omega_n'$ .

The complex representation (12a), which is formally simpler, is used in the present work.

### Application to Accelerator Mode

#### Formulation for Computing

We assume that the longitudinal field in the accelerating mode is transversely uniform near the axis, i.e.,

$$\psi_z \cong \psi_z(0, 0, \xi) \quad (13)$$

and note that the total beam current is given by

$$I(\tau) = \int_{\text{cav.}} J(\xi, \eta, \tau) d\xi d\eta \quad (14)$$

It will be convenient to introduce a new field variable  $W_n(\tau)$  defined as

$$\begin{aligned} W_n(\tau) e^{i\omega_n' \tau} & = -\frac{i\omega_n'}{c} \int_{\text{cav.}} A_{zn}(\tau + \xi/v_n) d\xi \\ & \cong \int_{\text{cav.}} E_z(\tau + \xi/v_n) d\xi \end{aligned} \quad (15)$$

That is,  $W_n$  is essentially the integral of electric field along an electron trajectory. Hence, the voltage gained by an electron passing through the  $n^{\text{th}}$  cavity at time  $\tau$  is

$$\Delta V_n(\tau) = \text{Re} \left( W_n(\tau) e^{i\omega_n' \tau} \right)$$

The complex voltage gain  $W_n(\tau)$  is assumed to be slowly varying in the sense that it changes by a negligible amount during the time,  $\ell/v_n$ , in which an electron passes through one cavity.

With the substitution of (13), (14) and (15) in Eq. (12a) the wave equation becomes

$$\frac{\partial W_n(\tau)}{\partial \tau} = \sum_{j=n-1}^{n+1} R_n^j W_j(\tau) + S_n(\tau) \quad (16)$$

where  $R_n^{n\pm 1} \equiv -\frac{i}{2} \frac{F_n}{F_{n\pm 1}} \Omega_n^{n\pm 1} e^{\mp i\omega' \ell / v_n}$  (17)

$$R_n^n \equiv -\alpha_n^{-i(\omega' - \omega_n)} \quad (18)$$

$$S_n(\tau) \equiv -\frac{\omega'}{\omega_n} \frac{2\pi |F_n|^2}{u_n} I(\tau) e^{-i\omega' \tau} \quad (19)$$

$$F_n \equiv \int_{\text{cav.}} \psi_{zn}(0, 0, \xi) e^{i\omega' \xi / v_n} d\xi \quad (20)$$

The voltage gain of the kth beam bunch in passing through the structure is given by

$$V(kt_b) = \text{Re} \sum_{n=0}^N W_n(kt_b) e^{ik\omega' t_b} \quad (21)$$

where  $t_b = 1/f_b$  is the bunching period and N is the total number of cavities.

The beam interaction source term (19) may be written in the alternate form

$$S_n(\tau) = -\alpha_n r_n \ell I(\tau) e^{-i\omega' \tau} \quad (19')$$

by use of a standard definition of  $r_n$ , the shunt impedance per unit length.

### Computer Program

A program for numerical solution of Eq. (16) has been written. The computational method is a typical (4th order) Runge-Kutta integration of the differential equation with appropriate tests for convergence and selection of more or less optimum time step. The integration is found to become unstable if the time step is such that

$$\Delta \tau \gtrsim 1/\Omega$$

Physically, this limit is equivalent to the group propagation time per cavity at the midband group velocity.

Data input options provide for description of waveguide structures having arbitrary variations of the parameters from cavity to cavity. Arbitrary driving source terms equivalent to constant voltage of constant current generators may be simulated in selected cavities. These sources may be turned on and off at preselected times with either a step-function or exponentially damped rise.

Boundary options equivalent to mid-cavity or mid-iris electric or magnetic shorting planes, or mid-iris

"infinite impedance" planes, are provided. These conditions, expressed for example at the input boundary, are

$$A_{-1}(\tau) = \pm A_0(\tau) \quad (\text{mid-iris shorting plane})$$

$$A_{-1}(\tau) = \pm A_1(\tau) \quad (\text{mid-cavity shorting plane})$$

and

$$A_{-1}(\tau) = 0 \quad (\text{mid-iris "infinite impedance" plane})$$

in which the + sign refers to electric and the - sign to magnetic planes. The boundary conditions at the output end are analogous.

The beam model parameters include time on, time off, rise time, beam frequency, and beam current.

Longitudinal dynamics are ignored in this program; the beam velocity is taken as  $v = c$ . Thus phase oscillations and possible longitudinal instabilities are not included.

### Typical Computations for the SLAC Structure

The SLAC waveguide<sup>12</sup> is a disc-loaded structure designed for approximately constant gradient when lightly beam-loaded. The operating mode is  $2\pi/3$ , traveling wave, at 2856 MHz. All the properties--group velocity, midband frequency, Q, and shunt impedance--vary practically linearly from input to output. The total number of cavities per 10-ft. section is 86. Figure 3 shows the Brillouin diagrams corresponding to several points along the structure and the following table summarizes the pertinent initial and final values of the parameters.

Cav. No.	$v_g/c$	$\Omega$	Q	r
0	.0204	32.0 MHz	14,170	0.53 MΩ/cm
85	.0061	10.41	13,220	0.60

The values of half-bandwidth,  $\Omega_n$ , used in the computation, are derived from the design group velocity,  $v_g(n)$ , through the relation

$$v_g = \frac{\partial \omega}{\partial k} \approx \Omega \ell \sin k\ell$$

Since the parameters vary adiabatically, we take  $\Omega_n^{\pm 1} = \Omega(n \pm 1/2)$ .

Figures 4 through 7 illustrate propagation of a step-function driving voltage applied at time  $\tau = 0$  at the input boundary. Note the appearance of increasing group dispersion at large n (compare Figs. 5 and 6) and the ripples resulting from the filter response of the periodic structure. Some of the more persistent wiggles, which are especially prominent in Fig. 5, result from the fact that the pass-band becomes narrower as n increases. Consequently, certain frequency components which are shock-excited by the step-function driving voltage are reflected from the 0- or  $\pi$ -mode band limit at some point down the structure, propagate back to the input where they are again reflected by the source boundary (constant voltage--i.e., zero impedance) and thus set up standing wave resonances. Such resonances probably would be much less noticeable in a more realistic case with finite rise-time and source impedance matched to the guide.

The appearance of a significant out-of-phase component of the field (Figs. 4, 5, 6) results from a slight

error, of  $\sim 0.06$  MHz, in entering the midband frequency of the structure. As a result the wave is not quite synchronous at the assumed bunching frequency of 2856 MHz.

#### Beam Loading Example

Figure 8 shows the voltage loss which is self-induced in a SLAC 10-ft. accelerator section by a step function beam current of 60 mA. The waveguide parameters are the same as in the previous examples.

The nominal steady state beam loading energy loss is  $\sim 2$  MeV per 10-ft. section at 60 mA pulse current.

#### Beam Blowup

##### Computational Method

**Formulation of blowup for computing.** In the case of beam blowup, the field is presumed to be the HEM<sub>11</sub> deflecting mode.<sup>3</sup> We consider a particular polarization, in the X-direction. Near the axis the longitudinal field is of the form

$$A_z \cong A_n(\tau) \xi \psi_n^{(1)} \quad (22)$$

where  $\psi_n^{(1)} = \frac{\partial \psi_z}{\partial \xi}$  evaluated at  $(0, 0, \xi)$ .

The beam current is given by  $J = \rho(x_n - \xi, y_n - \eta) I(\tau)$  where  $x_n$  and  $y_n$  are the coordinates of the beam centroid, and the transverse extent of the distribution function  $\rho$  is assumed to be small.

The right-hand side of Eq. (12), the beam interaction source term, now becomes

$$-\frac{2\pi ic}{\omega_n' u_n} \int_{\text{cav.}} \psi_{zn}^* J e^{-i\omega_n' \xi / v_n} dV = -\frac{2\pi ic}{\omega_n' u_n} F_n' * I(\tau) x_n(\tau) \quad (23)$$

where we redefine the cavity form factor as

$$F_n' = \int_{\text{cav.}} \psi_n^{(1)}(\xi) e^{i\omega_n' \xi / v_n} d\xi \quad (24)$$

To introduce beam dynamics into the picture, we note that the canonical momentum gained by a particle in a (vector) electromagnetic field is<sup>21</sup>

$$\Delta p_x = \frac{e}{c} \int_{(e)} \frac{\partial A_z}{\partial x} dz \quad (25)$$

and the displacement in the x direction is

$$\Delta x = \int_{(e)} \left( p_x - \frac{e}{c} A_x \right) \frac{dz}{p_z} \quad (26)$$

(the integral  $\int_{(e)}$  is along a particle trajectory).

It is usually assumed that the  $A_x$  term in Eq. (26) makes a negligible contribution to the displacement. This is certainly good in an impulse approximation through a short structure, but may not be valid in

extended structures at low beam energies. For the present we neglect the  $A_x$  term and say with reservations that

$$\Delta x \cong \int_{(e)} p_x dz / p_z \quad (26')$$

We now introduce the definitions

$$G_n(\tau) e^{i\omega' \tau} \equiv \int_{\text{cav.}} A_n(\tau + \xi / v_n) \psi_n^{(1)}(\xi) d\xi \quad (27)$$

$$x_n \equiv X_n(\tau) e^{i\omega' \tau} \quad (28)$$

$$p_{xn} \equiv P_n(\tau) e^{i\omega' \tau} \quad (29)$$

Note that  $(e/c)G_n(\tau)e^{i\omega' \tau}$  is the transverse momentum gain per cavity for an electron at time  $\tau$ . As before,  $\omega'$  is a constant reference frequency and the functions  $G_n(\tau)$ ,  $P_n(\tau)$ , and  $X_n(\tau)$  are assumed to be relatively slowly varying, e.g., do not contain frequency components much greater than the pass band width. Combining Eqs. 23 and 27 with 12 and including the beam dynamics, we obtain the blowup equations

$$\frac{\partial G_n(\tau)}{\partial \tau} = \sum_{j=n-1}^{n+1} R_n^j G_j(\tau) - i C_n I(\tau) X_n(\tau) \quad (30)$$

$$P_{n+1/2}(\tau) = P_{n-1/2}(\tau) + \frac{e}{c} G_n(\tau) \quad (31)$$

$$X_{n+1/2}(\tau) = X_{n-1/2}(\tau) + \frac{\ell}{p_{zn}} P_n(\tau) \quad (32)$$

in which

$$R_n^{n\pm 1} \equiv -\frac{i}{2} \frac{F_n'}{F_{n\pm 1}'} \Omega_n^{n\pm 1} e^{\mp i\omega' \ell / v_n} \quad (33)$$

$$R_n^n \equiv -\alpha_n - i(\omega' - \omega_n) \quad (18)$$

$$C_n \equiv \frac{2\pi c}{\omega_n' u_n} \frac{|F_n'|^2}{u_n} \quad (34)$$

and  $F_n'$  is defined by Eq. (24). The coefficient  $C_n$  may be expressed in the alternate form

$$C_n = \alpha_n r_{t,n} \ell \frac{\omega_n}{c} \quad (34')$$

where  $r_t$  is the transverse shunt impedance per unit length as defined by Altenmueller *et al.*<sup>22</sup>

**Limitations imposed by complex beam dynamics.** It is important to realize that the complex formulation of the beam dynamics, used in the present work, contains the implicit assumption that the beam charge is uniformly distributed as a function of rf phase angle. If the beam is bunched at some frequency related to the blowup frequency in a ratio of small integers, then the

complex representation of  $x$  and  $p_x$  is not valid. One such ratio occurs, in the SLAC case, at a frequency of 4284 MHz (equal to 3/2 times 2856), which happens to have phase velocity of  $c$  at about 7.5 ft. from the beginning of the 10 ft. structure. Experimentally, however, the SLAC blowup occurs at about 4140 MHz and computational results given in the next sections of the present paper indicate that the interaction strength becomes rather weak at frequencies much different from 4140. Thus although these interference effects still invite study with a formulation which takes them into account, the indications are that they will not be very important to the SLAC problem.\*

Another limitation of the complex representation is that non-linear beam transport elements such as sextupole lenses cannot be included. Both this and the interference phenomena mentioned above would require, essentially, ray-tracing each beam bunch through the structure. A computer program now being developed by Rees and Herrmannsfeldt<sup>23</sup> will be able to handle these effects, at least in the isolated-cavity blowup model equivalent to the Panofsky-Sessler formula- tion.<sup>18,19</sup>

### Computer Program

A program for numerical solution of the blowup Eqs. (30), (31), and (32) has been written. The wave propagation program described in the previous section is used, with suitable modification of the interaction term and simultaneous solution of the beam dynamics.

Provisions have been made for drift spaces, focusing lenses,\*\*and acceleration, by obvious generalizations of the beam dynamics equations; namely, the effect of a thin lens of focal length  $f$  is

$$\Delta P_n = -p_{zn} X_n / f$$

and the effect of a drift space (possibly with acceleration, but without transverse forces) is

$$\Delta X_n = P_n \int_{z_{n-1/2}}^{z_{n+1/2}} d\xi / p_z$$

Data input options allow arbitrary configuration of drift spaces, lenses and acceleration.

The effect of the blowup mode on the longitudinal dynamics is ignored. All beam particles are assumed to have the same longitudinal momentum, independent of time.

### Blowup Interaction Within the 10-ft. Accelerator Section

#### Properties of the Mode

Figure 9 shows typical Brillouin diagrams for the HEM<sub>11</sub> mode in different parts of the SLAC 10-ft.

\* See also the work of Gluckstern and Butler,<sup>9</sup> in which it is shown in a similar type of computation that the blowup is only enhanced by about a factor of two even in the "resonant" case where  $\omega_b = \omega_n$ .

\*\* Solenoid focusing has not been included. This would introduce coupling between  $x$  and  $y$  motions and require fields of both polarizations.

structure. The simple cosine dispersion curve, Eq.(8) shown for comparison, obviously does not fit the experimental data over the entire band, especially at the input end. The problem may be treated in an approximate way by fitting the parameters  $\omega_n$  and  $\Omega_n$  within a limited frequency range, and considering different frequency bands separately. This technique should be reasonably quantitative so long as we do not try to treat very rapid transients.

In the following calculations a fit which is valid from about 4120 to 4160 MHz is used. This corresponds to the range of synchronous frequencies within about the first 25 cavities of the SLAC structure (see Fig. 9).

The  $Q$  of the deflecting mode in a structure similar to the SLAC accelerator has been measured<sup>24</sup> as approximately 10,000. The shunt impedance has not been measured directly. Evaluation of the integrals in Eq. (34), on the assumption of a simple TM<sub>110</sub> cavity mode, leads to values of  $r_t/Q \approx 10 \Omega/cm$ . Indirect determination of  $r_t/Q$  from the observed blowup, by a method mentioned later in this report, gives  $r_t/Q \approx 12 \pm 2 \Omega/cm$ .

In the sample computations discussed below, the values used are  $Q = 10,000$  and  $r_t/Q \approx 10$  to  $12 \Omega/cm$ .

### Computed Resonances

The experiments of Farinholt et al.<sup>11</sup> have shown that the SLAC blowup occurs at a sharply defined frequency even though synchronism of the HEM<sub>11</sub> phase velocity with the electron velocity can occur over a band of more than 200 MHz. This blowup frequency has been identified as a standing wave resonance which occurs in the first few cavities of the SLAC accelerator pipe. That such resonances must exist may be seen from Fig. (9b), which shows that near the input end of the accelerator guide certain frequencies may be trapped between the  $\pi$ -mode stop band and the input coupler, which is a purely reactive load to the HEM<sub>11</sub> mode at a particular polarization.

These resonances have been probed by a series of computer runs simulating excitation of the accelerator guide by a beam having constant amplitude of transverse modulation, at an energy high enough so that negligible deflection takes place. By comparing the transverse momentum impulse at resonance, with the impulse generated by a single resonant cavity of the same  $r_t$  and  $Q$ , we can compute the effective interaction length.

Figure 10 shows the field distribution at several of these resonant modes, and the following table lists the first five modes with experimental frequencies<sup>25</sup> listed for comparison.

Computed Resonant Frequency	Experimental	Computed Effective Interaction Length
4139.4 MHz	4139.64 MHz	23.2 cm
4147.8	4147.50	8.9
4154.5	4154.00	11.2
4160.5	4159.72	8.1
4165.7	4164.82	8.1

### Suppression of Blowup Interaction by an External Load

One obvious means of reducing the blowup interaction would be to couple the power out of the

accelerator guide into a matched load, using a coupler which is below cutoff at the accelerating frequency. A computation was performed simulating a characteristic impedance termination at about the third cavity. The effect was to reduce the induced transverse impulse and field amplitude by more than a factor of 10, more or less independent of frequency, from the value found at the dominant resonance (4139.4 MHz). In an actual experiment<sup>11</sup> performed with a section of accelerator guide in which signals were induced by the partially blown-up beam of the SLAC accelerator, the load reduced the induced field by about a factor of 3. The uncertainties in performing the actual experiment were rather large.

Regenerative Blowup

A series of computer experiments have been performed to investigate the threshold for regenerative blowup in a single section of the SLAC structure. The procedure was to apply a very short pulse of transverse modulation to the beam and note the subsequent growth or decay of the fields and beam deflections at various currents.

Figure 11 shows the growth of the fields in the accelerator guide at 1 ampere pulse current under conditions approximating the SLAC injector;  $v/c = 0.75$  at injection, with acceleration at 0.1 MeV/cm. The field distribution corresponds closely to one of the resonant modes of the initial part of the tapered structure,\* and the natural frequency at which the blowup develops (4147.5 MHz) is quite close to the frequency of this resonance (4147.8 MHz). The small frequency shift of -0.3 MHz evidently corresponds to the optimum phase slippage between the beam and the wave<sup>4,5,6</sup> in this particular case. It is a little surprising that the natural blowup is not in the 4139.4 or the 4154.5 MHz modes, both of which have larger effective interaction lengths than the 4147.8 MHz mode. Presumably the low injection velocity ( $v/c = 0.75$ ) prevents the necessary degree of synchronism with the lower mode, which occurs nearer the beginning of the guide. In the case of the higher mode at 4154.5 MHz, which extends further into the guide, the interaction is perhaps damped by the rapid increase in rigidity of the accelerating beam.

Figure 12 shows growth of the deflection of the beam after passing through the interaction region, at several currents. Figure 13 shows the growth rate (inverse of e-folding time) as a function of current.

Blowup in the Multi-Section Machine

Analytic Predictions

The blowup observed at SLAC as described by Farinholt et al.,<sup>11</sup> results basically from a mechanism whereby a transverse modulation of the beam, starting initially from some sort of noise, is repeatedly amplified in successive accelerator sections until eventually the amplitude equals the accelerator aperture and the beam is lost.

The fact that the effect takes place at a unique and sharply defined frequency led Panofsky<sup>18</sup> and Sessler<sup>19</sup> to formulations in which the interaction in each accelerator section is treated as a single resonant "cavity" (actually, as we have seen, a standing wave resonance involving several cavities).

\* See "Computed Resonances," above.

In Panofsky's formulation, the successive impulses imparted by each "cavity" are treated in a continuous force approximation, resulting in a blowup equation which in the terminology of the present paper is given by

$$\left(\frac{\partial}{\partial \tau} + \alpha\right) \frac{\partial}{\partial z} \left(\gamma \frac{\partial X}{\partial z}\right) = -iC I_0 X \tag{35}$$

where

$$C = \frac{e}{mc^2} \frac{2\pi^2 c r_t \ell_1}{\lambda_0^2 L Q}$$

Here  $\gamma$  is the beam energy,  $L$  is the spacing between "cavities,"  $I_0$  is the pulse beam current,  $\lambda_0 = 2\pi c/\omega_0$ , and  $\ell_1$  is the effective length of the resonant interaction. This result follows readily from the present blowup Eqs. (30), (31), and (32) if we take the reference frequency as  $\omega' = \omega_0$ , set the inter-cavity coupling terms equal to zero, and identify  $nL$  as  $z$  in the continuous limit.

Asymptotic<sup>18</sup> and numerical<sup>26</sup> solutions of Eq. (35) have been found. The asymptotic result is of the form

$$X \sim \exp\left\{\frac{3}{2^{2/3}} e^{i\pi/6} (C I_0 \tau)^{1/3} \left(\int_0^z \frac{dz'}{\sqrt{\gamma(z')}}\right)^{2/3} - \alpha \tau - \frac{1}{4} \log \frac{\gamma}{\gamma_0}\right\} \tag{36}$$

To the extent that the decay term and the logarithmic term may be ignored, this implies a scaling law, in the case of constant acceleration, of

$$\frac{r_t \ell_1}{Q} \cdot \frac{I_0 \tau z}{(d\gamma/dz)} \approx \text{const.}$$

for given amplification of  $X$ . Panofsky<sup>18</sup> has estimated that an amplification of  $\sim e^{20}$  could result with typical SLAC parameters.

Panofsky also extended his equation to include focusing but was unable to obtain analytic results except in the case of very weak focusing. It appeared, however, that an appreciable increase in beam current should be possible.

The computer program has been used to probe the properties of the long accelerator blowup in the isolated cavity model, with emphasis on the improvement in beam current which could be expected from use of more and stronger focusing.

Typical Results on Long-Linac Blowup

Figure 14 shows the growth of the blowup in the SLAC machine as a function of time and distance, at a particular beam current, with no focusing. The starting condition is a constant amplitude of transverse modulation applied at  $z = 0$ . The beam is accelerated from an initial 30 MeV to 16.25 GeV.

In this computation and those which follow, not every individual "cavity" is included; instead, groups of several (4 to 16) accelerator sections are represented by a single cavity of appropriate effective length. The saving in computer time is impressive and the accuracy of the computation is found to be affected very little.

Determination of Effective  $r_t \ell_1/Q$

An experiment was performed by R. Miller (reported by Farinholt et al.<sup>11</sup>) in which the amplitude

of the transverse modulation was measured as a function of beam current and distance along the accelerator. By simulating the same experiment on the computer and fitting the results to the measured data it was possible to estimate (a) the parameter  $r_t \ell_1 / Q$  and (b) the amount of amplification required to produce pulse shortening. This is possible because the only sensitive unknown parameters in the experiment are  $(r_t \ell_1 I_0 / Q)$  [see i. e., Eqs. (30), (31), (32), or Eq. (35)], and the initial amplitude of  $X$ .\*

As a result of this calibration it is found that

$$r_t \ell_1 / Q = 280 \pm 50 \text{ ohm/10 ft. section}$$

Use of the effective interaction length of 23 cm (see "Computed Resonances," above) then gives

$$r_t / Q \approx 12 \pm 2 \Omega / \text{cm}$$

The amplification from the 30 MeV point (beginning of Sector 1) to produce pulse shortening at  $1.5 \mu\text{sec}$  is found to be in the range of  $1 \cdot 10^6$  to  $2.5 \cdot 10^7$  with a nominal value of  $4 \cdot 10^6$ . (Figure 15.)

#### Improvement of Beam Current by Focusing

The SLAC focusing system<sup>27</sup> at present consists of a quadrupole multiplet lens at the end of every sector (333-1/3 ft.) and an additional weaker lens at the 40 ft. point in Sector 1.

From the point of view of blowup suppression we would like to set all the lenses for maximum admittance of the system, corresponding to focal length of a half-sector (4 lenses per betatron wavelength). That is, because of the relation

$$\text{multiplet focal length} \sim \gamma^2 / I_Q^2$$

where  $I_Q$  is quadrupole current, we should taper the quadrupole currents in proportion to beam energy.

The present lenses can be run at strengths corresponding to maximum admittance at energies of up to only about 7 GeV, or 1/3 of the machine. In the paper of Farinholt et al.,<sup>11</sup> a plan for up-grading the focusing system is outlined. In Phase I of the plan, provisions will be made for continuing the maximum admittance lens setting throughout the machine. Phase II calls for additional lenses in the first part of the machine, at closer spacing. This will allow stronger focusing in the low energy region where the rate of growth of the blowup is most rapid.

Figure 16 shows schematically the two phases of the quadrupole plan. Figure 17 illustrates the sort of beam current improvement to be expected on the basis of the computer calculation. The Phase II model assumed for these computations has 4 multiplet lenses per sector for the first 6 sectors, and one per sector thereafter. The improvement factors appear to be about 1.6 for Phase I and 2.6 for Phase II.

#### Improvement by RF Suppression

The blowup interaction might be significantly reduced, e.g., by use of external loads as discussed earlier in this report, or by tuning the structures so

\* The starting noise may depend somewhat on beam current, but this would bias the  $r/Q$  calibration only slightly because of the extremely rapid dependence of amplification on beam current.

that the resonances would be displaced in some random or systematic manner from section to section. A computer experiment was carried out, assuming that the interaction strength was decreased by a factor of 10 in the first two sectors. The beam current improvement factor in this case seems to be about 1.25.

#### Time Varying Quadrupoles

Several computer runs were made in which some of the quadrupoles were modulated at frequencies of a few megacycles. The thought here was that, if the betatron phase of the transverse modulation could be shifted appreciably during the buildup time of the blowup, the coherence of the signal arriving at a given point along the machine would be partially destroyed.

The computations indicated that this mechanism would be quite ineffective. The maximum reduction in blowup amplification obtained under physically realistic conditions was on the order of a factor of 2, as compared to factor of  $\sim 10^6$  required to produce pulse shortening. The beam current improvement would then be expected to be no more than  $\sim 20\%$ . The problem is that, on one hand, it is necessary to introduce appreciable betatron phase shift within each e-folding distance along the machine, but on the other hand it is impossible to modulate any one lens by a very large percentage because the resulting over- or under-focusing would tend to make the blowup worse. Since the e-folding distance under blowup conditions can be on the order of one sector or less, the ineffectiveness of this scheme is not surprising.

#### Acknowledgements

The author is indebted to E. L. Chu, R. Miller, G.A. Loew, J. Haimson, W.K.H. Panofsky, W.B. Herrmannsfeldt, J. Rees and M. Sands for stimulating discussions.

The computational work was performed on the Burroughs B5500 and IBM 7090 computers at the Stanford University Computation Center.

#### List of References

1. M.C. Kelliher and R. Beadle, "Pulse Shortening in Electron Linear Accelerators," *Nature* **187**, 1099 (1960).
2. T.R. Jarvis, G. Saxon, M.C. Crowley-Milling, "Experimental Observations of Pulse Shortening in a Linear Accelerator Waveguide," *Proc. IEEE* **112**, No. 9 (1965).
3. H. Hahn, "Deflecting Mode in Circular Iris Loaded Waveguide," *Rev. Sci. Instr.* **34**, 1094 (1963).
4. H. Hirakawa, "Pulse Shortening Effect in Linear Accelerators," *Jap. J. Appl. Phys.* **3** (No. 1), 27 (1964).
5. P.B. Wilson, HEPL Report No. 297, High Energy Physics Laboratory, Stanford University, Stanford, California.
6. G.H.H. Chang, "Pulse Shortening in Electron Linear Accelerators," M. Sc. Thesis, University of California, Berkeley, California (1964); see also E. L. Chu, SLAC Internal Report TN-66-17, Stanford Linear Accelerator Center, Stanford, California (1966).
7. J. E. Bjorkholm and R.F. Hyneman, "An Analysis of TM<sub>11</sub> Mode Beam Blowup in Linear Accelerators," *IEEE Trans. Electron Devices*, p. 281 (May 1965).

8. R.L. Gluckstern and H.S. Butler, "Transverse Beam Blowup in a Standing Wave Linac Cavity," IEEE Trans. Nucl. Sci. NS-12 (No. 3), 607 (1965).
9. M.C. Crowley-Milling, "A 40-MeV Electron Accelerator for Germany," AEI Engineering 2, No. 2 (1962).
10. A.K. Valter, et al., "2-GeV Traveling Wave Electron Accelerator," International Accelerator Conference, Frascati (1965).
11. E.V. Farinholt, Z.D. Farkas, W.B. Herrmannsfeldt, H.A. Hogg, R.F. Koontz, C.J. Kruse, G.A. Loew, and R.H. Miller, "Beam Breakup Experiments at SLAC," LASL Linac Conference, Los Alamos, New Mexico (1966), p. 267.
12. A.L. Eldredge, G.A. Loew, and R.B. Neal, "Design and Fabrication of the Accelerating Structure for the Stanford Two-Mile Accelerator," SLAC Report No. 7, Stanford Linear Accelerator Center, Stanford, California (1962).
13. L. Brillouin, Wave Propagation in Periodic Structures, (McGraw-Hill, Inc., New York, 1946).
14. J.C. Slater, Microwave Electronics, (D. Van Nostrand, Inc., New York, 1950); Chap. IV.
15. R.M. Bevensee, Electromagnetic Slow Wave Systems (John Wiley and Sons, Inc., New York, 1964).
16. D.E. Nagle, "Coupled Resonator Model of Linear Accelerator Tanks," Minutes of 1964 Conference on Proton Linear Accelerators, MURA-714, p. 21, (1964).
17. T. Nishikawa, "Normal Mode Analysis of Standing Wave Linacs—Field Excitation and Beam Loading in Linac Cavities," BNL Internal Report AADD-87, Brookhaven National Laboratory, Lepton, New York (1965).
18. W.K.H. Panofsky, "Transient Behavior of Beam Breakup," SLAC Internal Report TN-66-27, Stanford Linear Accelerator Center, Stanford, California (1966).
19. A. Sessler, Lecture given at the Stanford Linear Accelerator Center, May 26, 1966 (unpublished).
20. J.E. Leiss and R.A. Schrack, "Transient and Beam Loading Phenomena in Linear Electron Accelerators," NBS Internal Report, Washington, D.C. (October 30, 1962).
21. W.K.H. Panofsky, and W.A. Wentzel, Rev. Sci. Instr. 27, 967 (1956).
22. O.H. Altenmueller, R.R. Larsen, and G.A. Loew, "Investigations of Traveling Wave Separators for the Stanford Two-Mile Linear Accelerator," SLAC Report No. 17, Stanford Linear Accelerator Center, Stanford California (1963).
23. J. Rees and W.B. Herrmannsfeldt, private communications.
24. J. Haimson, private communication. The author thanks Dr. Haimson for permission to use unpublished data on the Q of the HEM<sub>11</sub> mode.
25. O.H. Altenmueller, private communication. The author thanks Mr. Altenmueller for his kindness in measuring the resonant frequencies in the SLAC accelerator guide.
26. M. Bander "Solution of the Beam Break-up Equation," SLAC Internal Report TN-66-28, Stanford Linear Accelerator Center, Stanford, California (1966).

27. R.H. Helm, "Optical Properties of Quadrupole Multiplets for Sector Focusing in the Two-Mile Accelerator," SLAC Report No. 14, and "Misalignment and Quadrupole Error Problems Affecting the Choice of Multiplet Type for Sector Focusing of the Two-Mile Accelerator," SLAC Report No. 15, Stanford Linear Accelerator Center, Stanford, California (1963).

The present list of references on the subjects of linac beam blowup, beam loading, and coupled resonator theory is in no sense complete; the author hopes that the titles cited are reasonably representative.

†Work supported by the U. S. Atomic Energy Commission.

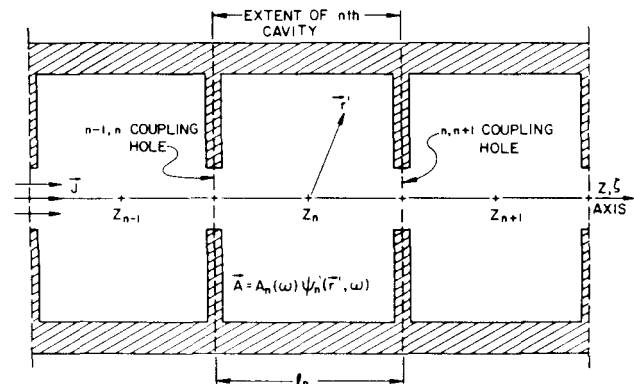


Fig. 1. Schematic representation of coupled cavity chain. The local coordinate system in the nth cavity is  $\vec{r}' = (\xi, \eta, \zeta)$ .

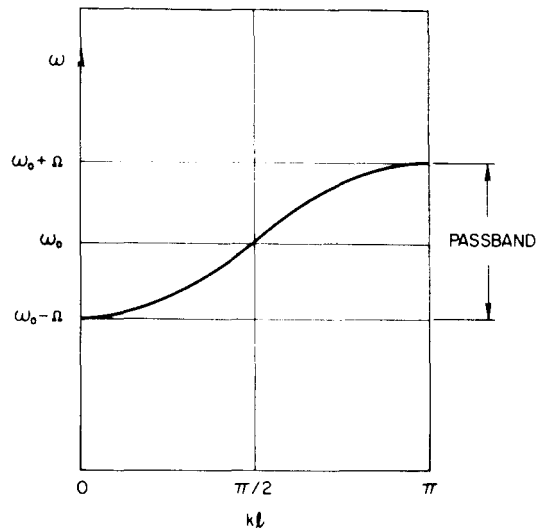


Fig. 2. "Ideal" Brillouin diagram corresponding to the simple dispersion formula  $\omega_0 + ia - \omega = \nu \cos kl$  (Eq. 8).

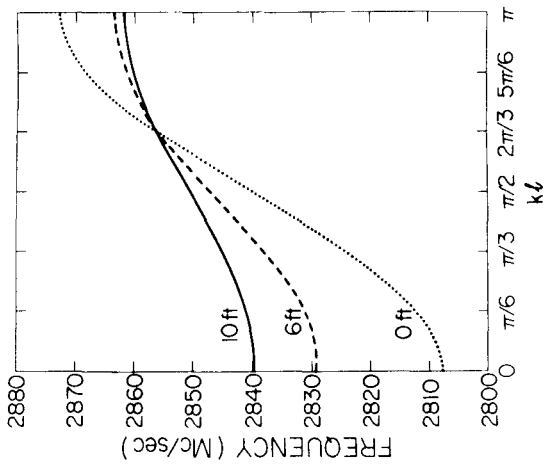


Fig. 3. Typical Brillouin diagrams for the accelerating mode in the SLAC structure.

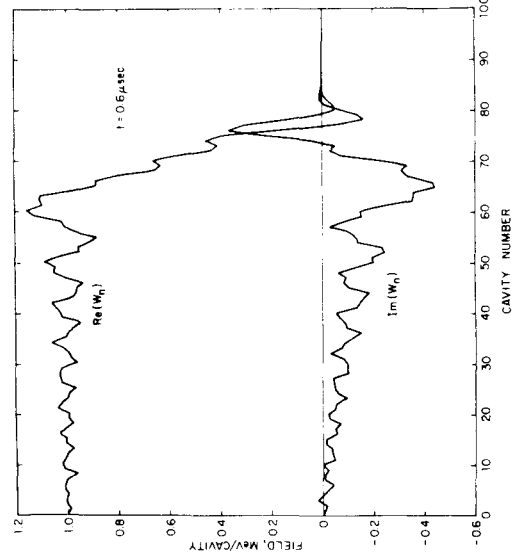


Fig. 4. Field distribution in the accelerating mode along SLAC constant-gradient structure 0.6  $\mu$ sec after turning on a unit step-function driving voltage in the 0-th cavity.

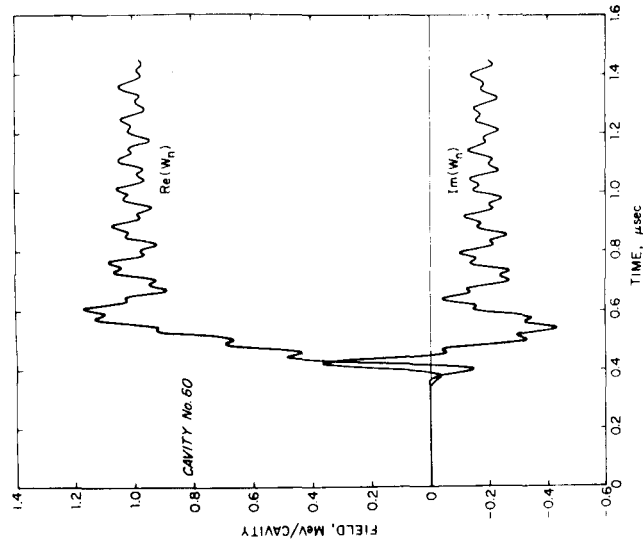


Fig. 5. Arrival of the rf pulse at cavity No. 60 (6.9 ft point).

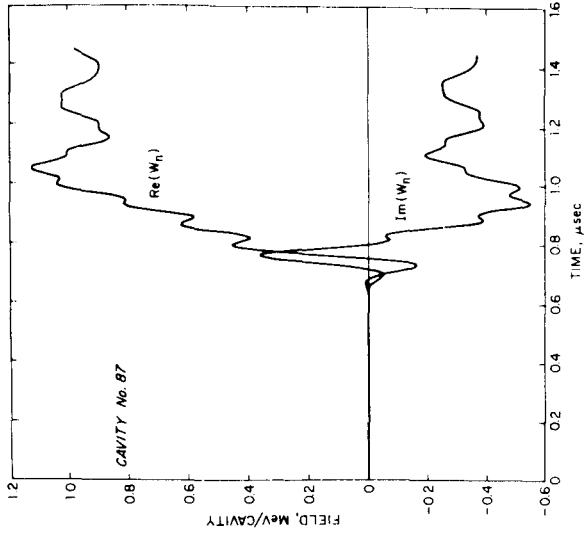


Fig. 6. Arrival of the rf pulse at the 10-ft point. Note increased dispersion of the initial rise, as compared to Fig. 5. The substantial out-of-phase component results from an error of  $\sim 0.06$  MH in entering the midband frequency in the program input data.

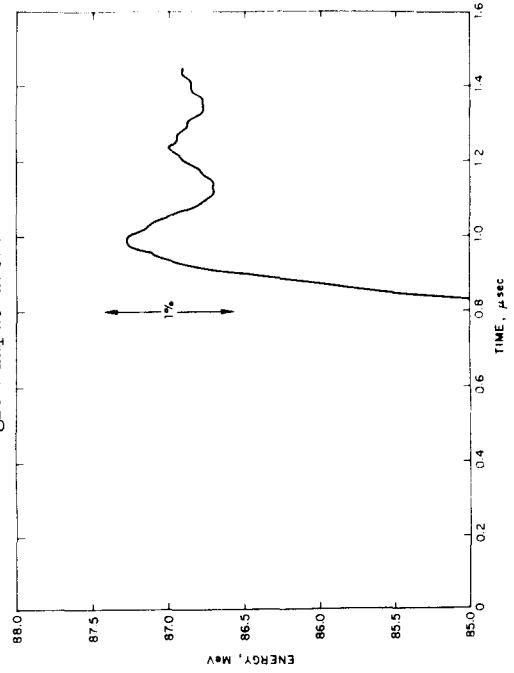


Fig. 7. Electron energy gain vs time corresponding to the case of Figs. 4-6. The large ripples seen in the field plots have nearly averaged out in the summation over the cavities.

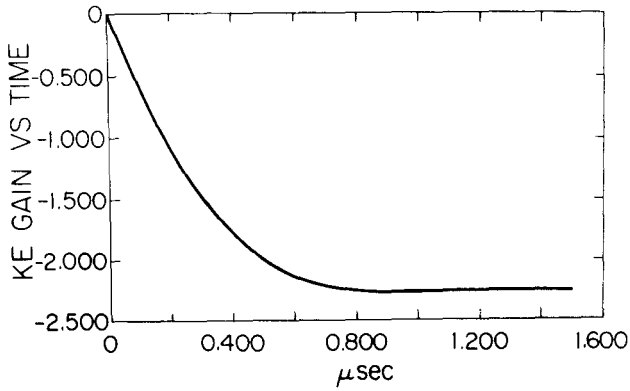


Fig. 8. Self-induced energy loss in SLAC structure in the accelerating mode by a stip-function beam current of 60 mA.

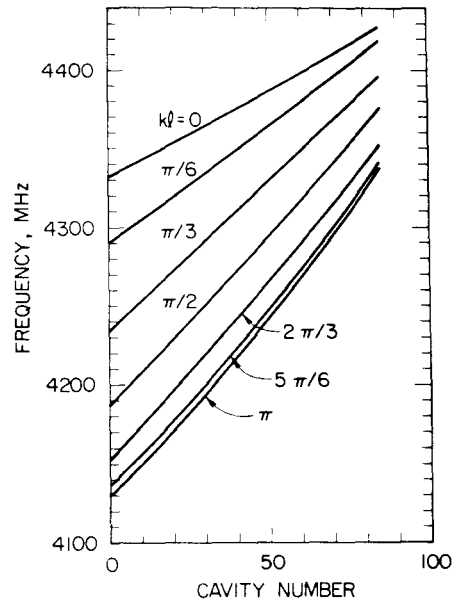
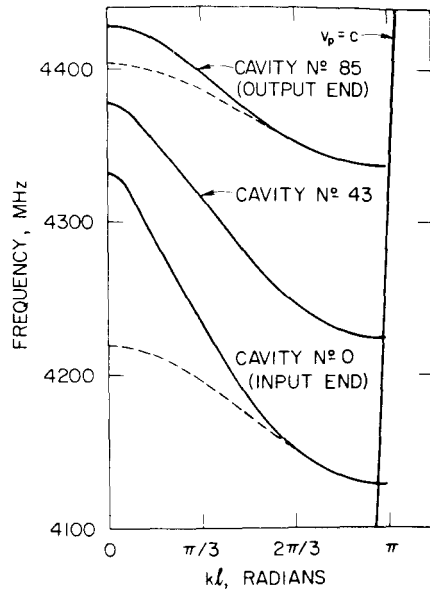
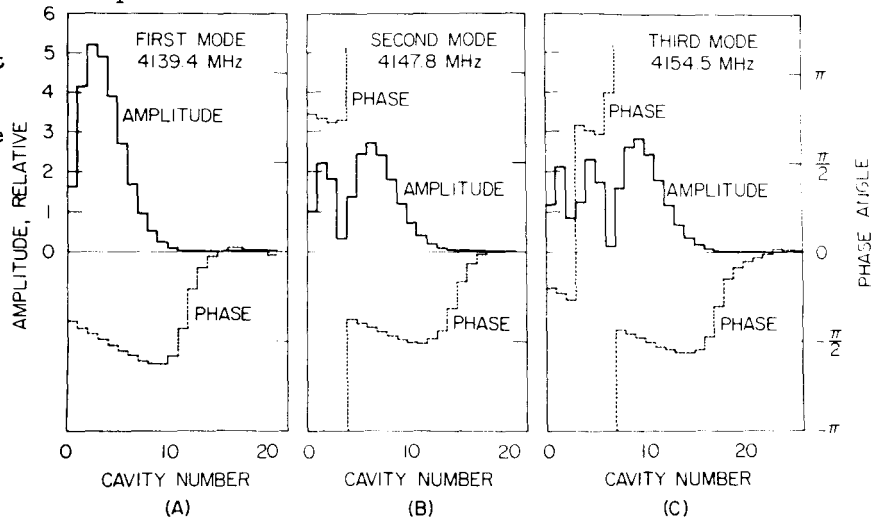


Fig. 9a. Brillouin diagrams for  $HEM_{11}$  (deflecting) mode at input end, middle and output end of SLAC structure. Solid curves are measured data and dashed curves are simple dispersion formula (Eq.8), fit to the measured data near synchronous point ( $v_p + c$ ).

Fig. 9b. Same data as 9a, plotted as  $\omega$  vs  $n$  with  $kl$  as a parameter. The synchronous condition  $v_p + c$  occurs very close to  $\pi$ -mode over the entire length.

Fig. 10 a,b,c. Computed field distribution of first three  $HEM_{11}$  resonant modes in SLAC guide. The quantity plotted is  $G_n(\tau)$ , the transverse momentum impulse per cavity (Eq. 27). The phase angle is relative to the beam transit angle. The excitation is by a beam at low current and high energy with a uniform transverse modulation which changes negligibly in amplitude in going through the interaction region. Conditions: Beam current  $I_0 = 50$  mA; beam energy  $V = 100$  MeV;  $Q = 10,000$ ;  $\tau = 2.0$   $\mu$ sec =  $1.5 \cdot (2Q/\omega)$ ;  $r_t = 0.12$  M $\Omega$ /cm.



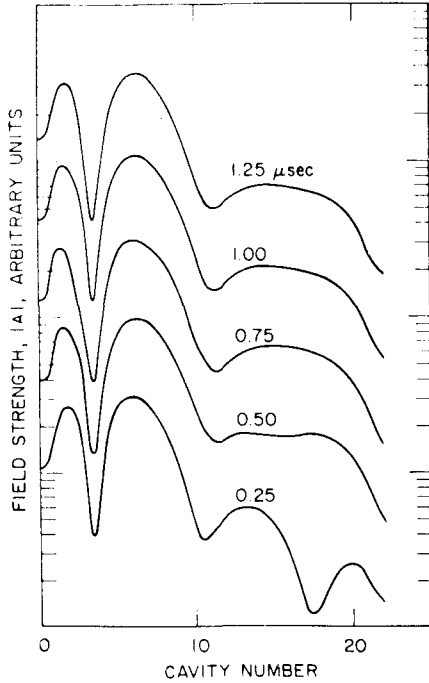


Fig. 11. Growth of field during regenerative blowup. The quantity plotted is  $|G_n|$  or  $|A_n|$ . Conditions:  $I_0 = 1$  amp; injection energy = 260 KeV ( $v/c = 0.75$ ); acceleration = 0.1 MeV/cm;  $Q = 10,000$ ;  $r_t = 0.12$  MΩ/cm. The starting signal is a delta function impulse of transverse modulation. The blowup takes place at a natural frequency of 4147.5 MHz.

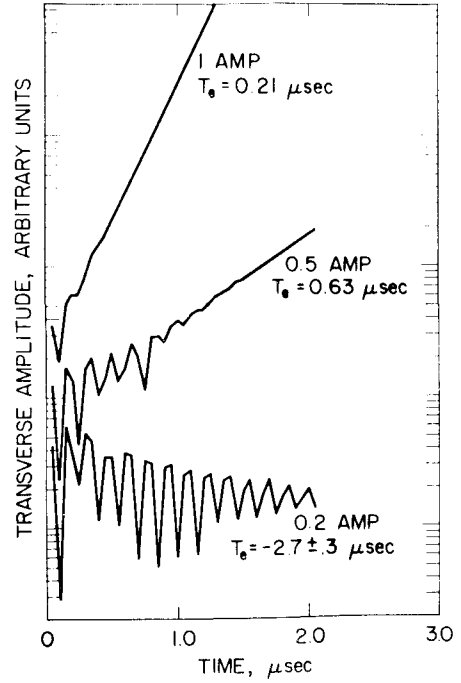


Fig. 12. Growth of beam deflection during regenerative blowup at several currents. Conditions: same as for Fig. 11.

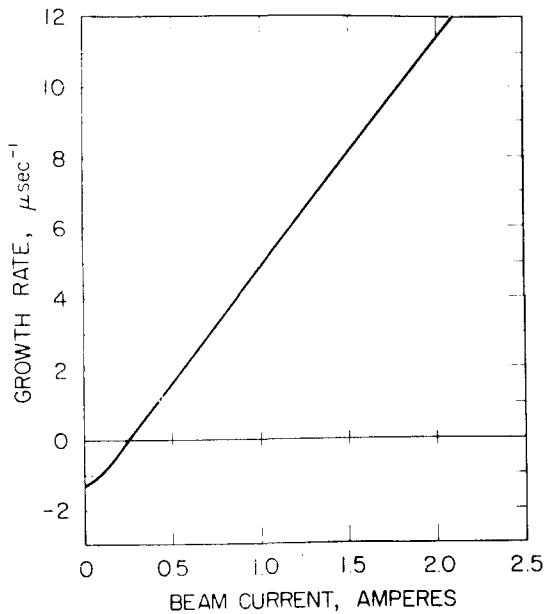


Fig. 13. Exponential buildup rate of regenerative blowup, as a function of beam current. Conditions: same as Fig. 11.

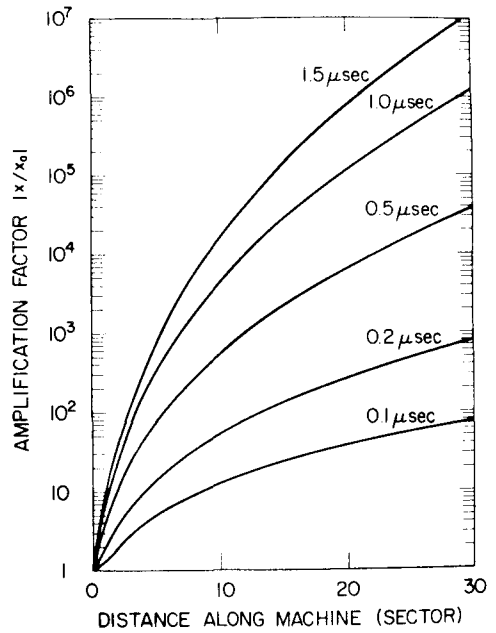


Fig. 14. Growth of beam deflection during SLAC type blowup (isolated cavity model<sup>10</sup>). Conditions:  $I_0 = 10$  mA; initial energy = 30 MeV; approx. uniform acceleration to 16.25 GeV final energy;  $Q = 10,000$ ;  $r_t l_1 = 2.5$  MΩ/10-ft.section; no focusing. (Note: One sector = 32 10-ft. sections.)

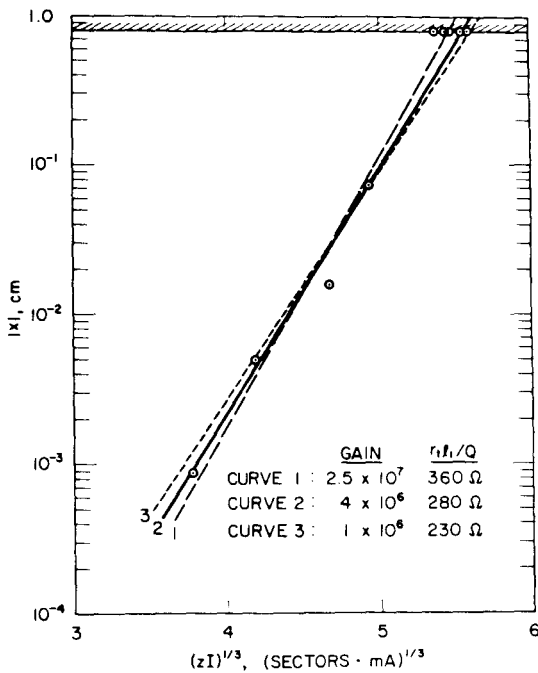


Fig. 15. Experimental determination of  $r_t l_1 / Q$  and gain. The experimental points represent a measurement of blowup amplitude at  $\tau = 1.5 \mu\text{sec}$  as a function of beam current and distance along the machine. It is assumed that  $Q = 10,000$  but the exact value affects the result only slightly. The functional dependence of amplitude on  $(zI)$  is approximate. The value of  $r_t l_1 / Q$  used in the computation is scaled to fit the shape of the curve; normalization then gives the gain required to amplify the initial noise to blowup amplitude ( $\sim 0.8 \text{ cm}$ ). The gain is based on injection at 30 MeV with constant amplitude of transverse modulation.

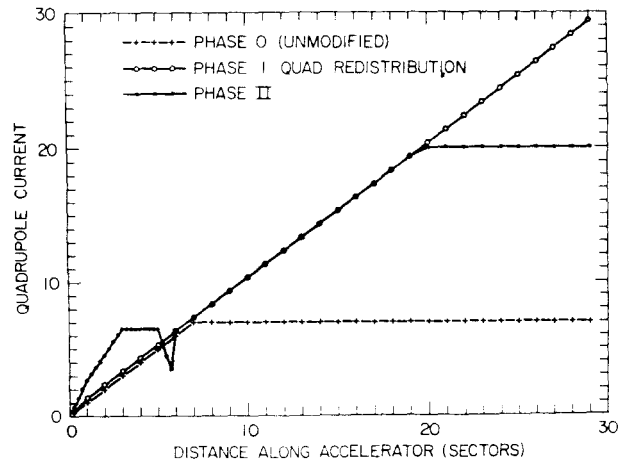


Fig. 16. Schematic layout of focusing schemes. Each point represents a quadrupole doublet. The ordinate is a measure of focal strength, proportional to quadrupole current.

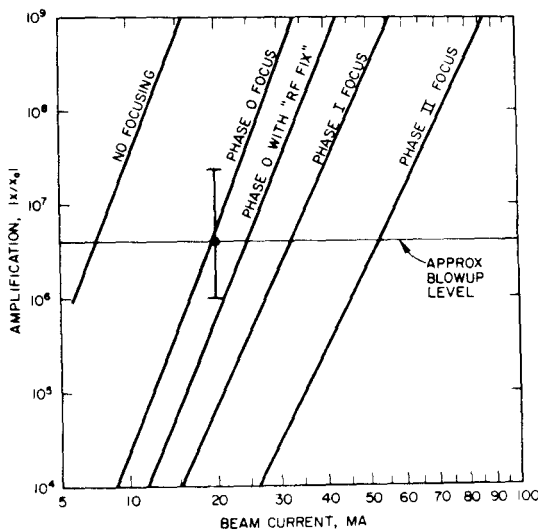


Fig. 17. Amplification (gain) at sector 30 vs beam current for SLAC type blowup. Conditions: Injection at 30 MeV with constant amplitude transverse modulation; uniform accelerator to 16.25 GeV;  $\tau = 1.5 \mu\text{sec}$ ;  $Q = 10,000$ ;  $r_t l_1 = 2.8 \text{ M}\Omega / 10\text{-ft. section}$ . Phase 0, I and II focusing schedules as in Fig. 16. The curve labeled "rf fix" assumes suppression of the blowup interaction in sectors 1 and 2. The circled point at 20 mA near the "phase 0" curve is essentially the maximum current which has been obtained experimentally.